Geophys. J. Int. (2003) **152,** 669–676

Finite-frequency resolution limits of wave path traveltime tomography for smoothly varying velocity models

Jianming Sheng and Gerard T. Schuster

Department of Geology and Geophysics, University of Utah, Salt Lake City, UT 84112, *USA. E-mail: schuster@mines.utah.edu*

Accepted 2002 September 23. Received 2002 August 19; in original form 2002 January 17

SUMMARY

The Rytov approximation that expresses phase residuals as an explicit function of the slowness perturbations, is also related to the generalized Radon transform (GRT). Using Beylkin's formalism, we derive the corresponding *inverse* GRT to give the slowness model as an explicit function of the phase residuals. This expression is used to deduce the resolution limits of wave path traveltime tomograms as a function of source frequency and source–receiver geometry. Its validity is restricted to arbitrary models with smooth variations in velocity, where the scale wavelength of the velocity variations must be at least three times longer than the characteristic source wavelength. The formula explicitly gives the slowness perturbation function as a function of the product of the frequency and the traveltime gradient that can be obtained by ray tracing. It shows that the spatial resolution limits of a slowness anomaly can be estimated by calculating the available wavenumbers of the slowness perturbation function. Using this procedure, resolution limits are obtained for several types of data: controlled source data in a crosswell experiment, data from a diving-wave experiment and earthquake data using the reference velocity model of the whole Earth. This formula can also be used for diffraction-limited pixelization of velocity models or for direct inversion of traveltime data.

Key words: seismic resolution, tomography, traveltime.

1 INTRODUCTION

Current 3-D models of the whole Earth are primarily based on velocity images calculated by tomographic inversion of earthquake traveltimes. Such models have revolutionized our understanding of the Earth's origins, convection cells and tectonic mechanisms (e.g. Dziewonski 1984; Su *et al.* 1994; Ritsema *et al.* 1999). However, tomographic images are limited in accuracy because the high-frequency assumption of ray theory conflicts with the inherent low frequency of the observed teleseismic arrivals. This conflict leads to an inaccurate estimate of the model errors because the finite-frequency effects are not taken into account (Tong *et al.* 1998; Marquering *et al.* 1999).

Exploration seismologists also use ray-based tomographic methods to determine subsurface velocity structures, and so their velocity models are also limited by finite-frequency effects in the data. With few exceptions, tomographers generally ignore the wave-interference effects that can significantly limit the resolution of their tomographic images.

To correct this deficiency, Woodward & Rocca (1988); Woodward (1989, 1992) and Luo & Schuster (1990, 1991) developed inversion methods that accounted for finite-frequency effects in body wave traveltime data under the Rytov and Born approximations, respectively. Instead of backprojecting traveltime residuals along raypaths, Woodward and Rocca's formulation backprojected phase residuals along Rytov wave paths in the space–frequency domain while Luo & Schuster backprojected traveltime residuals along Born wave paths in the space–time domain. In either case, the finite-frequency effects of wave propagation were partly accounted for and led to more accurate tomograms with low-frequency data. Here, the region of a first-Fresnel zone or wave path is defined by the following condition (Kravtsov & Orlov 1980):

$$|\tau(\mathbf{r}', \mathbf{r}_s) + \tau(\mathbf{r}', \mathbf{r}_g) - \tau(\mathbf{r}_s, \mathbf{r}_g)| \leq \frac{T}{2}, \tag{1}$$

where T is the period, $\tau(\mathbf{r}, \mathbf{r}')$ is the traveltime for waves to propagate from $\mathbf{r}$ to $\mathbf{r}'$, and the point $\mathbf{r}'$ belongs to the first-Fresnel zone for the source–receiver pair $(\mathbf{r}_s, \mathbf{r}_g)$ if and only if it satisfies eq. (1).

The problem with wave-equation methods is that they are usually too expensive to routinely implement, particularly with earthquake-tomography studies where the teleseismic waves have propagated over thousands of kilometres. A cheaper, but less effective, means of accounting for wave-interference effects in traveltime tomograms is to derive resolution limits based on wave path effects, and to incorporate these into estimates of model variances for ray-based tomograms (Schuster 1996; Wu & Toksoz 1987).

Now, we derive such resolution limits for traveltime tomograms computed for arbitrary Earth models with smooth variations in the velocity. The starting point is to relate the phase to the model using the Rytov approximation, recognize the resulting equation as a

generalized Radon transform (GRT), and use Beylkin's (1985) formalism to derive the inverse GRT. The inverse GRT explicitly represents the slowness model as a function of phase data, and shows that the wavenumber of the slowness anomaly can be estimated as the product of the frequency and the traveltime gradient, so that resolution limits of the reconstructed slowness model can be obtained. These limits are valid in the asymptotic high-frequency limit, but are still useful for finite-frequency phenomena. To paraphrase Bleistein (1984): '... the results of the asymptotic analysis are usually meaningful when the typical wavelength is (in practice three times or more) shorter than the typical dimension in the problem'. Velocity images obtained by earthquake traveltime tomography, reflection traveltime tomography or diving-wave tomography can now be assessed for their limits of resolution based on the finite-frequency effects of the data and smoothly varying velocity models.

This paper is divided into three parts. The first section presents the derivation of the inverse GRT formula that explicitly relates the reconstructed model to the phase data. From this formula we derive the resolution limits of the slowness model as a function of source frequency and source–receiver coverage. The second section presents some numerical examples where the resolution limits are computed for a crosswell experiment, a diving-wave experiment and whole-Earth tomography. Finally, the conclusions are presented.

2 THEORY

Under the first-order Rytov approximation the wavefield-phase residual $\Delta\phi(\omega, \mathbf{r}_s, \mathbf{r}_g) = \ln[\psi(\omega)] - \ln[\psi_0(\omega)]$ can be linearly related to the object function $\mathbf{O}(\mathbf{r})$ as (Woodward 1992)

$$\Delta\phi(\omega, \mathbf{r}_s, \mathbf{r}_g) = \int \mathbf{O}(\mathbf{r})\omega^2 \frac{G_0(\omega, \mathbf{r}, \mathbf{r}_s)G_0(\omega, \mathbf{r}, \mathbf{r}_g)}{G_0(\omega, \mathbf{r}_s, \mathbf{r}_g)}\, d\mathbf{r}, \tag{2}$$

where ψ and ψ_0 are the perturbed and background wavefields, respectively; G_0 represents the Green's function for the background model and the support of $\omega^2[G_0(\omega, \mathbf{r}, \mathbf{r}_s)\, G_0(\omega, \mathbf{r}, \mathbf{r}_g)]/G_0(\omega, \mathbf{r}_s, \mathbf{r}_g)$ defines the region of the Rytov wave path; $\mathbf{r}_s$ and $\mathbf{r}_g$ denote the source and geophone locations; the object function is given as $\mathbf{O}(\mathbf{r}) = 1/[V^2(\mathbf{r})] - 1/[V_0^2(\mathbf{r})]$; and $V_0(\mathbf{r})$ denotes the background velocity.

Using the first term of the geometrical optics approximation, the Green's function can be written as

$$G_0(\omega, \mathbf{r}, \mathbf{r}') = -\exp\left[-\frac{i(n+1)\pi}{4}\right]\omega^{(n-3)/2} a_0(\mathbf{r}, \mathbf{r}')\mathrm{e}^{i\omega\tau_0(\mathbf{r}, \mathbf{r}')}, \tag{3}$$

where n denotes the model dimension; $a_0(\mathbf{r}, \mathbf{r}')$ and $\tau_0(\mathbf{r}, \mathbf{r}')$ satisfy the transport and eikonal equations, respectively.

Substituting eq. (3) into eq. (2) and equating imaginary parts of both sides of eq. (2), the imaginary part of $\Delta\phi(\omega, \mathbf{r}_s, \mathbf{r}_g)$ yields the time-delay-like phase delay and can be linearly related with the object function $\mathbf{O}(\mathbf{r})$ as

$$\mathrm{Im}[\Delta\phi(\omega, \mathbf{r}_s, \mathbf{r}_g)] = -\int_{\mathbf{X}} \omega^{(n+1)/2}\mathbf{O}(\mathbf{r})A(\mathbf{r}, \mathbf{r}_s, \mathbf{r}_g) \times \sin\left[\omega\tau(\mathbf{r}, \mathbf{r}_s, \mathbf{r}_g) - \frac{(n+1)\pi}{4}\right] d\mathbf{r}, \tag{4}$$

where $A(\mathbf{r}, \mathbf{r}_s, \mathbf{r}_g) = [a_0(\mathbf{r}, \mathbf{r}_s)a_0(\mathbf{r}, \mathbf{r}_g)]/a_0(\mathbf{r}_s, \mathbf{r}_g)$ represents the geometrical spreading term of the Rytov wave path, $\mathbf{X}$ denotes the model domain and $\tau(\mathbf{r}, \mathbf{r}_s, \mathbf{r}_g) = \tau_0(\mathbf{r}, \mathbf{r}_s) + \tau_0(\mathbf{r}, \mathbf{r}_g) - \tau_0(\mathbf{r}_s, \mathbf{r}_g)$.

According to Beylkin's theory, eq. (4) can be related to a causal GRT, and the asymptotic inverse formula in the case of a fixed source can be expressed as (see Appendix A)

$$\mathbf{O}^{\mathrm{est}}(\mathbf{r}) = -\frac{4}{(2\pi)^n}\int_\omega\int_{\partial\mathbf{X}} \omega^{(n-3)/2}\,\mathrm{Im}[\Delta\phi(\omega, \mathbf{r}_s, \mathbf{r}_g)] \times \sin\left[\omega\tau(\mathbf{r}, \mathbf{r}_s, \mathbf{r}_g) - \frac{(n+1)\pi}{4}\right] \times \frac{h(\mathbf{r}, \mathbf{r}_s, \mathbf{r}_g)}{A(\mathbf{r}, \mathbf{r}_s, \mathbf{r}_g)}\chi(\mathbf{r}, \mathbf{r}_s, \mathbf{r}_g)\, d\mathbf{r}_g\, d\omega, \tag{5}$$

where $\partial\mathbf{X}$ denotes the model boundary, $h(\mathbf{r}, \mathbf{r}_s, \mathbf{r}_g)$ is Beylkin's determinant (Beylkin 1985)

$$h(\mathbf{r}, \mathbf{r}_s, \mathbf{r}_g) = \begin{vmatrix} \partial_{r_1}\tau & \partial_{r_2}\tau & \cdots & \partial_{r_n}\tau \\ \partial_{r_1 r_{g_1}}\tau & \partial_{r_2 r_{g_1}}\tau & \cdots & \partial_{r_n r_{g_1}}\tau \\ \vdots & \vdots & \ddots & \vdots \\ \partial_{r_1 r_{g_{n-1}}}\tau & \partial_{r_2 r_{g_{n-1}}}\tau & \cdots & \partial_{r_n r_{g_{n-1}}}\tau \end{vmatrix}, \tag{6}$$

and $\chi(\mathbf{r}, \mathbf{r}_s, \mathbf{r}_g)$ is a cut-off function chosen to ensure that $\chi(\mathbf{r}, \mathbf{r}_s, \mathbf{r}_g)$ $h(\mathbf{r}, \mathbf{r}_s, \mathbf{r}_g) \geq 0$ on $\mathbf{X} \times \partial\mathbf{X}$ (Beylkin 1985). Here, $\partial_{r_i}\tau = \partial\tau(\mathbf{r}, \mathbf{r}_s, \mathbf{r}_g)/\partial r_i$ and $\partial_{r_i r_{g_j}}\tau = \partial^2\tau\left(\mathbf{r}, \mathbf{r}_s, \mathbf{r}_g\right)/\partial r_i \partial r_{g_j}$.

When $\mathrm{Im}[\Delta\phi(\omega, \mathbf{r}_s, \mathbf{r}_g)] \approx \omega\Delta\tau$ (here $\Delta\tau$ is equal to the difference between the observed traveltime and the calculated traveltime) (Schuster & Quintus-Bosz 1993), eqs (4) and (5) can also be written as

$$\Delta\tau(\mathbf{r}_s, \mathbf{r}_g) = -\int_{\mathbf{X}} \omega^{(n-1)/2}\mathbf{O}(\mathbf{r})A(\mathbf{r}, \mathbf{r}_s, \mathbf{r}_g) \times \sin\left[\omega\tau(\mathbf{r}, \mathbf{r}_s, \mathbf{r}_g) - \frac{(n+1)\pi}{4}\right] d\mathbf{r}, \tag{7}$$

and

$$\mathbf{O}^{\mathrm{est}}(\mathbf{r}) = -\frac{4}{(2\pi)^n}\int_\omega\int_{\partial\mathbf{X}} \omega^{(n-1)/2}\Delta\tau(\mathbf{r}_s, \mathbf{r}_g) \times \sin\left[\omega\tau(\mathbf{r}, \mathbf{r}_s, \mathbf{r}_g) - \frac{(n+1)\pi}{4}\right] \times \frac{h(\mathbf{r}, \mathbf{r}_s, \mathbf{r}_g)}{A(\mathbf{r}, \mathbf{r}_s, \mathbf{r}_g)}\chi(\mathbf{r}, \mathbf{r}_s, \mathbf{r}_g)\, d\mathbf{r}_g\, d\omega. \tag{8}$$

Eq. (5) or (8) can also be expressed as a Fourier transform (see Appendix A)

$$\mathbf{O}^{\mathrm{est}}(\mathbf{r}) = \frac{1}{(2\pi)^n}\int_{\Omega(\mathbf{r})} \mathrm{e}^{-i\mathbf{k}\cdot\mathbf{r}}\hat{\mathbf{O}}(\mathbf{k})\, d\mathbf{k}, \tag{9}$$

where $\hat{\mathbf{O}}(\mathbf{k})$ denotes the Fourier transform of $\mathbf{O}(\mathbf{r})$ and $\mathbf{k}$ is the wavenumber vector given by

$$\mathbf{k} = \omega[\nabla\tau_0(\mathbf{r}, \mathbf{r}_s) + \nabla\tau_0(\mathbf{r}, \mathbf{r}_g)], \tag{10}$$

where ω represents the source frequency; $\nabla\tau_0(\mathbf{r}, \mathbf{r}_s)$ and $\nabla\tau_0(\mathbf{r}, \mathbf{r}_g)$ are the gradients of the traveltimes; both $\tau_0(\mathbf{r}, \mathbf{r}_s)$ and $\tau_0(\mathbf{r}, \mathbf{r}_g)$ satisfy the eikonal equation and can be calculated by conventional ray tracing for a given velocity model and source–receiver geometry. In eq. (9), the integration domain $\Omega(\mathbf{r})$ is determined by the frequency range and by those source–receiver pairs $\eta_{sg}(\mathbf{r})$ for which the associated wave path and the recorded traveltimes can be influenced by the perturbation at $\mathbf{r}$.

The set $\Omega(\mathbf{r})$ in the Fourier domain determines the spatial resolution of the reconstructed object function $\mathbf{O}^{\mathrm{est}}(\mathbf{r})$ and controls what can be recovered (Beylkin 1985). As an example, the maximum value of k_x or k_z in the integration limits of eq. (9) determines the smallest resolvable features in the horizontal (i.e. Δx) and vertical (i.e. Δz) directions.

Therefore, the resolution limits of the wave path traveltime tomogram at some point $\mathbf{r}$ can be estimated as

$$\Delta x_i(\mathbf{r}) \approx \frac{\pi}{\max_{\eta_{sg}(\mathbf{r})T} k_{x_i}} = \frac{1}{2\max_{\eta_{sg}(\mathbf{r})T}\left[\left|\partial_{x_i}\tau_0(\mathbf{r},\mathbf{r}_g)+\partial_{x_i}\tau_0(\mathbf{r},\mathbf{r}_s)\right|\right]/T}, \quad (11)$$

where Δx_i is the resolution limit along the coordinate direction x_i, ∂_{x_i} denotes the derivative along the x_i coordinate and T is the minimum period of the data. For finite frequencies, the region in the vicinity of the raypath that mostly influences the recorded traveltime for a given source–receiver pair is usually denoted as the first-Fresnel zone of a wave path (Woodward 1989) or a Fresnel volume (Kravtsov & Orlov 1980; Červený & Soares 1992; Vasco *et al.* 1995); so $\eta_{sg}(\mathbf{r})$ represents the source–receiver pairs for which the point $\mathbf{r}$ is within the first-Fresnel zone of the corresponding wave paths.

As an example, energy that emanates from a scatterer at $\mathbf{r}$ will arrive at every receiver, but only when the scatterer is within the first-Fresnel zone of a reflection or transmission wave path can it influence the associated reflection or transmission traveltime. Thus the source–receiver pairs $\eta_{sg}(\mathbf{r})$ in eq. (11) are restricted to those wave paths that intersect the scatterer. This idea is illustrated in Fig. 1. The source–receiver pairs $\eta_{sg}(\mathbf{r})$ for reflection and transmission traveltime tomography are quite different, and this results in a different coverage for the wavenumbers of the reflection and transmission traveltime tomograms. Transmission traveltime tomography is usually associated with a narrower coverage of wavenumbers, and thus results in a poorer resolution in the transmission traveltime tomogram.

3 RELATIONSHIP TO MODEL RESOLUTION OPERATORS

Eq. (9) says that the estimated model is given by a blurred version of the actual model. The blurring kernel can be related to that of a model resolution kernel (Backus & Gilbert 1968) by inserting the identity

$$\hat{\mathbf{O}}(\mathbf{k}) = \int_{\mathbf{X}} \mathrm{e}^{i\mathbf{k}\cdot\mathbf{r}}\mathbf{O}(\mathbf{r})\,d\mathbf{r}, \quad (12)$$

into eq. (9) to obtain

$$\mathbf{O}^{\mathrm{est}}(\mathbf{r}) = \int_{\mathbf{X}'} G(\mathbf{r}\,|\,\mathbf{r}')\mathbf{O}(\mathbf{r}')\,d\mathbf{r}', \quad (13)$$

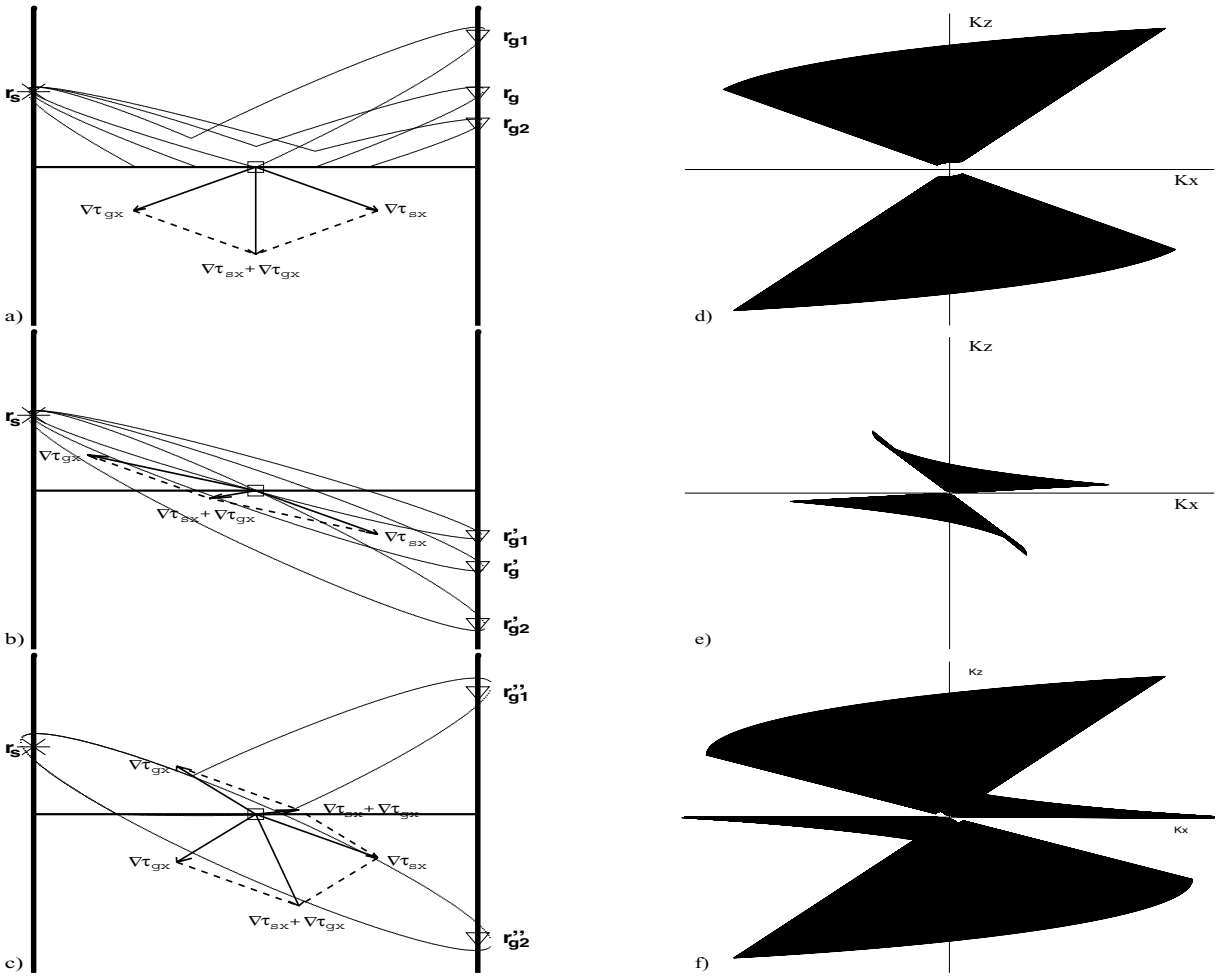

Figure 1. Crosswell geometry. (a) For a fixed source at $\mathbf{r}_s$ and a centred scatterer, the scattered energy will influence the reflection traveltimes observed at geophones $\mathbf{r}_g$ between $\mathbf{r}_{g1}$ and $\mathbf{r}_{g2}$, (b) the transmission traveltimes observed at geophones $\mathbf{r}'_g$ between $\mathbf{r}'_{g1}$ and $\mathbf{r}'_{g2}$, and (c) the diffracted traveltimes observed at all available geophones. The scatterer intersects the boundaries of the reflection wave paths associated with source–receiver pairs ($\mathbf{r}_s$, $\mathbf{r}_{g1}$) and ($\mathbf{r}_s$, $\mathbf{r}_{g2}$), and the transmission wave paths associated with ($\mathbf{r}_s$, $\mathbf{r}'_{g1}$) and ($\mathbf{r}_s$, $\mathbf{r}'_{g2}$), respectively. The source–receiver pairs ($\mathbf{r}_s$, $\mathbf{r}_g$) and ($\mathbf{r}_s$, $\mathbf{r}'_g$) define η_{sg} in eq. (9) for reflection and transmission traveltime wave path tomography, respectively; (d) The available wavenumbers for the reconstructed model for reflection traveltime wave path tomography, (e) transmission traveltime wave path tomography and (f) diffraction traveltime wave path tomography. Compared with that in (d) and (f), the wavenumber coverage in (e) is diminished, and thus results in a poorer vertical resolution for transmission traveltime wave path tomography.

where the blurring kernel $G(\mathbf{r} \mid \mathbf{r}')$ is given by

$$G(\mathbf{r} \mid \mathbf{r}') = \frac{1}{(2\pi)^n} \int_{\Omega(\mathbf{r})} e^{i\mathbf{k}\cdot(\mathbf{r}'-\mathbf{r})}\, d\mathbf{k}. \tag{14}$$

Therefore, the limits of resolution illustrated by, for example, the quadrilateral regions in Fig. 5 (see Section 4.3), delineate the support for the dominant part of the resolving kernel $G(\mathbf{r} \mid \mathbf{r}')$. The resolving kernel is also referred to as a point spread function for optical imaging (Jansson 1997), or a migration Green function for reflection imaging (Schuster & Hu 2000).

4 NUMERICAL EXAMPLES

Some numerical examples will now be computed for estimating slowness resolution limits for different types of seismic data: traveltime data from crosswell McElroy field data (Harris *et al.* 1992), traveltimes from diving waves and synthetic earthquake traveltimes for whole-Earth tomography.

4.1 CROSSWELL McElroy FIELD DATA

The resolution limits are estimated for wave path diffraction traveltime tomography and a 2-D crosswell data set, the McElroy data (Harris *et al.* 1992; Zhou *et al.* 1997). There are 201 shots evenly distributed along the well from depths of 811 to 963 m, with a source interval of 0.76 m. For each common shot gather, there are 186 hydrophones evenly distributed from depths of 822 to 963 m, with a trace interval of 0.76 m. The offset between the wells is 56 m, and the velocity model is discretized into a (295, 801) grid, with gridpoint intervals of 0.19 m. Fig. 2(a) shows the *p*-wave raypath traveltime tomogram. This tomogram has a vertical resolution of approximately 10 m in the centre of the model that corresponds to a reservoir sand unit, and it does not contain detailed information concerning the reservoir lithology. Taking this tomogram to be the background model and using eq. (11), the spatial resolution limits for transmission wave path traveltime tomography can be estimated for any scatterer. Figs 2(b)–(d) show the coverage of wavenumbers of the reconstructed slowness anomaly for the scatterers at an offset

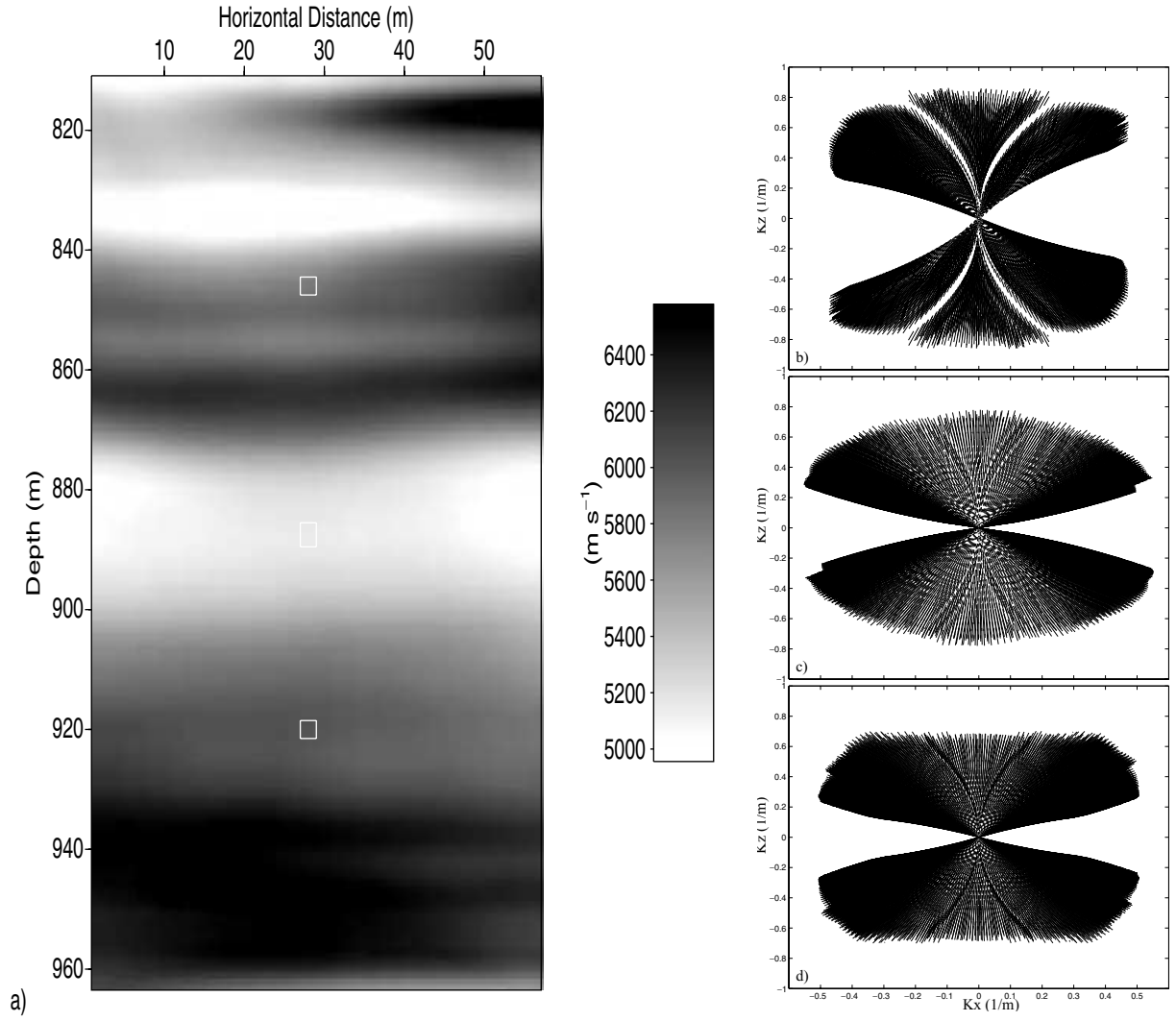

Figure 2. Traveltime tomogram reconstructed from crosswell McElroy field data (data courtesy of Harris *et al.* 1992). There are 201 shots evenly distributed along the well from depths of 811 to 963 m, and there are 186 hydrophones evenly distributed from depths of 822 to 963 m for each shot gather. The offset between the wells is 56 m, and the velocity model is discretized into a (295, 801) grid with gridpoint intervals of 0.19 m. (a) *P*-velocity traveltime tomogram. The three boxes represent three scatterers at the offset of $x = 28$ m, and at depths of 846, 887 and 920 m. The available wavenumbers for these three scatterers are shown in (b)–(d) suggesting that the estimated spatial resolutions (Δx, Δz) are (6.63, 3.65) m, (5.68, 4.03) m and (6.19, 4.48) m. Here, a maximum source frequency of 1400 Hz was assumed.

of $x = 28$ m, and at depths of 846.0, 887.0 and 920.0 m, respectively. The x- and z-direction resolution limits (Δx, Δz) can be estimated as (6.63, 3.65), (5.68, 4.03) and (6.19, 4.48) m. Zhou *et al.* (1997) showed that the vertical resolution of the McElroy traveltime tomogram can be improved to approximately 3 m or less by elastic traveltime and waveform inversion.

4.2 Diving-wave traveltime tomography

Sheriff & Geldart (1982) presented an analytical formula for the traveltime of the direct arrival for a $v(z)$ model with a linearly increasing velocity. We now use this formula to determine the spatial resolution limits of a traveltime tomogram for a linearly increasing velocity model. A model with a linear increase in velocity will be assumed with a and v_0 to be the velocity gradient and the surface velocity, respectively. The sources and receivers are continuously distributed from (0, 0) to (L, 0), as shown in Fig. 3. According to eq. (11), the spatial resolution limits for the scatterer at **x** in a diving-wave traveltime tomogram can be estimated by calculating the maximum wavenumbers $|k_x|$ and $|k_z|$ over those source–receiver pairs (**s**, **r**) for which the associated wave path includes **x**. For a fixed source at **s**, the maximum wavenumber can be calculated as (see Appendix B)

$$|k_x| \approx \pi \sqrt{\frac{8a}{(v^2 - v_0^2)T}} \sqrt{(1 - p^2v^2)\sqrt{1 - p^2v_0^2}}, \tag{15}$$

and

$$|k_z| \approx \pi \sqrt{\frac{8a}{(v^2 - v_0^2)T}} \sqrt{p^2v^2\sqrt{1 - p^2v_0^2}}, \tag{16}$$

where $p = (\sin i_0)/v_0$ defines the parameter for the raypath **sx**, i_0 is the take-off angle and v is the velocity at the image point (x, z). For a source at $\mathbf{s} = (x_s, 0)$ the ray parameter can be expressed as

$$p = \left[v_0^2 + \left\{ \frac{a\left[(x_s - x)^2 + z^2\right] + 2zv_0}{2|x_s - x|} \right\}^2 \right]^{-1/2}, \tag{17}$$

where x_s denotes the x-coordinate of the source at **s**. Since the receiver aperture is limited, only p-values that obey the following conditions should be considered:

$$0 \le x_s \le x - \frac{az^2 + 2zv_0}{a(L - x)} \tag{18}$$

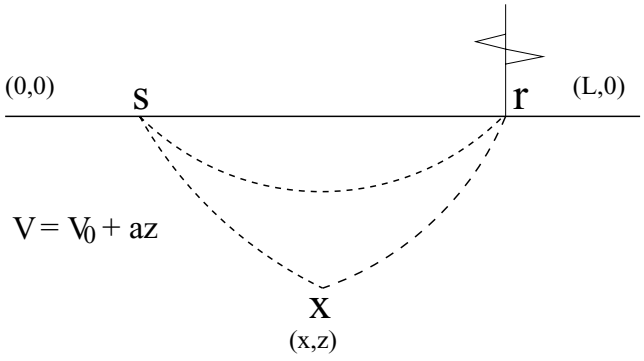

Figure 3. Diving-wave traveltime tomography. The velocity increases linearly with depth z, with a gradient a and the surface velocity v_0. The spatial resolution limits for a scatterer at **x** can be estimated by calculating the traveltime gradients $\nabla_{\mathbf{x}}(\tau_{\mathbf{sx}} + \tau_{\mathbf{xr}})$ when the scatterer is on the boundary of the diving-wave path for the source–receiver pair (**s**, **r**).

or

$$x + \frac{az^2 + 2zv_0}{ax} \le x_s \le L, \tag{19}$$

and the range of the p-value $[p_{\min}, p_{\max}]$ can be determined. Thus, the maximum wavenumbers from eqs (15) and (16) can be obtained, so that the spatial resolution limits can be estimated according to eq. (11).

In the case of unlimited aperture, when p approaches zero at the far-offset trace, the maximum value of $|k_x|$ in eq. (15) can be obtained as $\max|k_x| \approx \pi\sqrt{8a/(v^2 - v_0^2)T}$ and the x-direction resolution limit can be estimated as $\Delta x \approx \sqrt{[(v^2 - v_0^2)T]/8a}$. Similarly, when $z \le [(3 - \sqrt{6})/\sqrt{6}](v_0/a)$ and $p = \sqrt{6}/3v_0$, we have, $\max|k_z| \approx \pi\sqrt{8a/(v^2 - v_0^2)T}[(\sqrt[4]{12}/3)(v/v_0)]$ and $\Delta z \approx \sqrt{(v^2 - v_0^2)T/8a}[(3/\sqrt[4]{12})(v_0/v)]$; when $z \ge [(3 - \sqrt{6})/\sqrt{6}](v_0/a)$ and $p = 1/v$, we have, $\max|k_z| \approx \pi\sqrt{8a/(v^2 - v_0^2)}\,T\sqrt[4]{(v^2 - v_0^2)/v^2}$ and $\Delta z \approx \sqrt{(v^2 - v_0^2)T/8a}\sqrt[4]{v^2/(v^2 - v_0^2)}$.

4.3 Global earthquake tomography

Whole-Earth P-velocity tomograms can be obtained by inverting the first-arrival traveltimes picked from teleseismic records. Such tomograms are limited in resolution by the finite-frequency effects of low-frequency waves propagating through the Earth. To understand these limits we calculated the wave paths for 1 Hz teleseismic P waves.

The Preliminary Reference Earth Model or PREM (Dziewonski *et al.* 1981) is taken to be the background velocity model, and traveltimes are computed by an eikonal-equation solver. These traveltimes are then used to calculate numerically the wavenumber of the reconstructed model defined by eq. (10), and the spatial-resolution limits of the tomogram by eq. (11). Along a central ray, the wavenumber will be zero according to eq. (10) and this is consistent with the wave path theory (Woodward & Rocca 1988; Marquering *et al.* 1999). The sources and geophones are distributed uniformly around

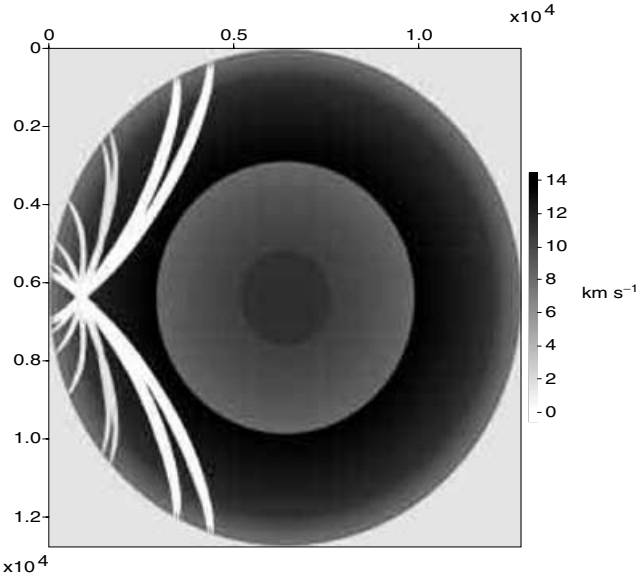

Figure 4. The transmission wave paths that intersect a single point at a depth of 800 km. The sources and receivers are distributed uniformly around a great circle of the Earth at a spatial interval of 1 degree for every source (or receiver), the dominant frequency is set to be 1 Hz, and the gridpoint interval is taken to be 2 km. The units of both the x-and z-coordinates are in km, and the units of velocity are km s^{-1}. The fat rays are the wave paths (Woodward & Rocca 1988; Luo 1991; Marquering *et al.* 1999).

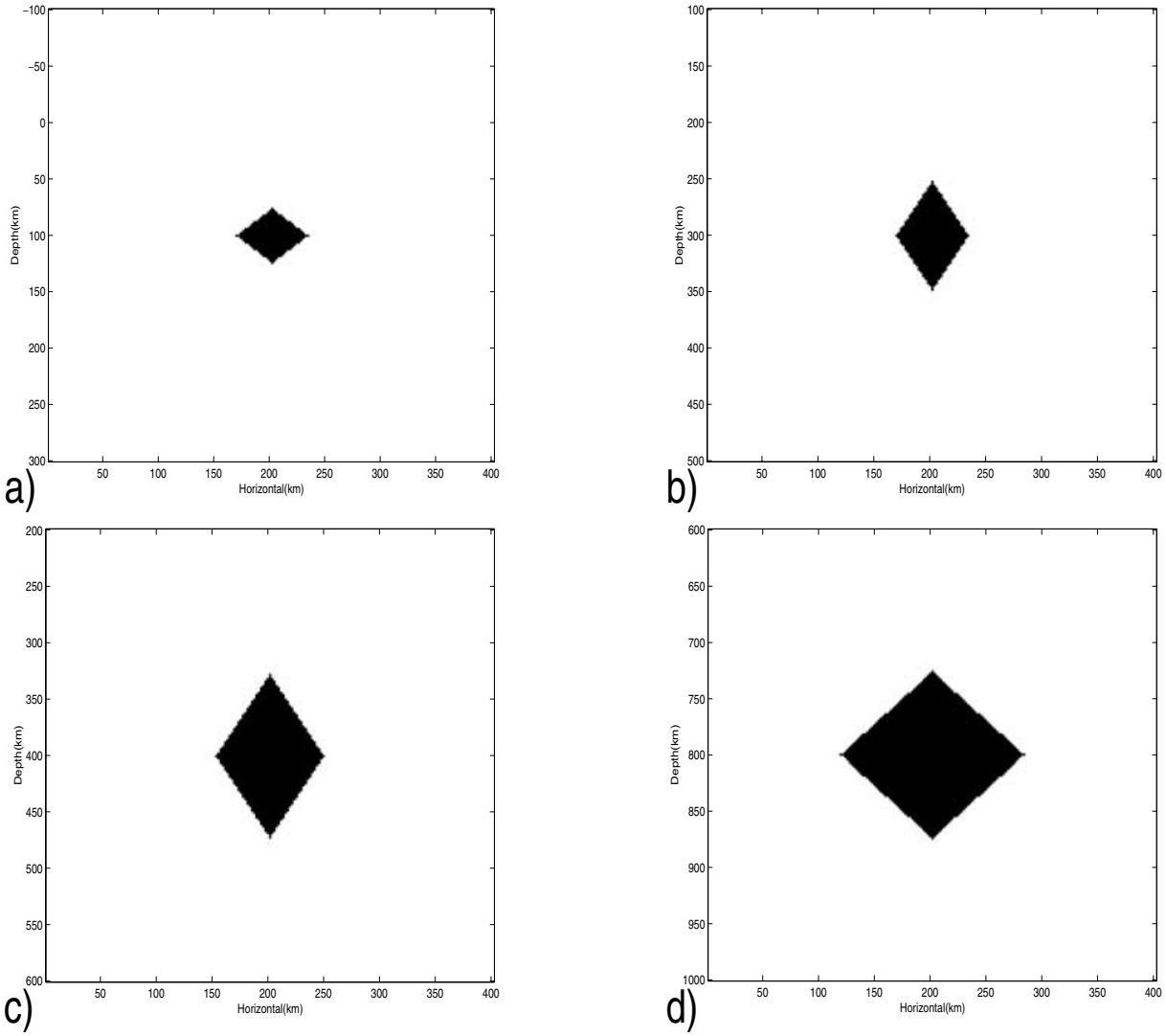

Figure 5. The unresolvable regions at different depths. The image points under consideration are at the centre of the quadrilaterals that represent the unresolvable regions. The size of the quadrilaterals gives the spatial resolution limits of an earthquake traveltime tomogram, where wave interference effects are partly taken into account. The horizontal width gives the horizontal resolution Δx and the vertical height gives the vertical resolution Δz. The sources and the geophones are uniformly distributed around a great circle of the Earth for 1 degree every source (or geophone). (a) Depth = 100, $\Delta x = 32$, $\Delta z = 24$ km; (b) depth = 300, $\Delta x = 32$, $\Delta z = 48$ km; (c) depth = 400, $\Delta x = 48$, $\Delta z = 72$ km; (d) depth = 800, $\Delta x = 82$, $\Delta z = 74$ km.

a great circle at a spatial interval of 1° for every source (or receiver); the dominant frequency is set to be 1 Hz and the gridpoint interval is taken to be 2 km.

Fig. 4 shows the wave paths superimposed on to the PREM, where only first-arrival traveltimes are used and we consider a region no deeper than 1500 km. Fig. 5 shows the approximated unresolvable regions for the scatterers at the depths of 100, 300, 400 and 800 km, respectively. The result shows that the spatial resolution generally becomes worse at deeper depths. At depths between 100 and 300 km, the spatial resolution (horizontal or vertical) is approximately 32 km, and between 400 and 900 km it is approximately 75 km.

5 CONCLUSIONS

We have derived the inverse GRT for the Rytov equation, which yields the reconstructed slowness as an explicit function of phase residuals. This formula also provides a practical means for estimating the limits of model resolution arising from wave-interference effects. It is valid for arbitrary Earth models with smoothly varying velocities having variations longer than three times the source wavelength. For the crosswell example, resolution formulae are derived that are in agreement with formulae derived under the far-field approximation. For the earthquake tomography example, a procedure is defined that allows for the computation of the wave path resolution limits of earthquake tomograms for given source–receiver geometries, image point locations and source frequencies. And for the diving-wave problem, simple formulae are given, which yield vertical- and horizontal-resolution limits of a diving-wave tomogram associated with a layered-Earth model.

One of the implications of this work is that the reliability estimates for global tomograms should take into account wave path resolution limits. This can be done by varying the size of the pixels in the tomographic velocity model so that they are no smaller than that dictated by the resolution limit, i.e. diffraction-limited pixelization of the model. A possible application of the inverse GRT formula is that it can be used as a fast means for inverting traveltime data.

ACKNOWLEDGMENT

We thank the sponsors of the 1999 University of Utah Tomography and Modelling/Migration Consortium (UTAM) for their financial support.

REFERENCES

Backus, G. & Gilbert, F., 1968. The resolving power of gross earth data, *Geophys. J. R. astr. Soc.,* **16,** 169–205.

Beylkin, G., 1985. Imaging of discontinuities in the inverse scattering problem by inversion of a causal generalized Radon transform, *J. Math. Phys.,* **26,** 99–108.

Bleistein, N., 1984. *Mathematical Methods for Wave Phenomena,* Academic Press, New York.

Červený V. & Soares E., 1992. Fresnel volume ray tracing, *Geophysics,* **57,** 902–915.

Dziewonski, A.M., Chou T.-A. & Woodhouse, J.H., 1981. Determination of earthquake source parameters from waveform data for studies of global and regional seismicity, *J. geophys. Res.,* **86,** 2825–2852.

Dziewonski, A., 1984. Mapping the lower mantle: Determination of lateral heterogeneity in *P*-velocity up to degree and order 6, *J. geophys. Res.,* **89,** 5929–5952.

Harris, J.M., Nolen-Hoeksema, R., Rector, J.W., Schaack, M.V. & Lazaratos, S.K., 1992. High-resolution crosswell imaging of a west Texas carbonate reservoir: Part 1. Data acquisition and project overview, *Expanded Abstracts of the 1992 Technical Programme of the Society of Exploration Geophysicists with Biographies,* pp. 35–39, Society of Exploration Geophysicists, Oklahoma, USA.

Jansson, P., 1997. *Deconvolution of Images and Spectra,* Academic Press, New York.

Kravtsov, Yu. A. & Orlov, Yu. I., 1980. Limits of applicability of the method of geometrical optics and related problems, reprinted in *Geometrical Aspects of Scattering*, ed. Marston, P., SPIE Milestone Series, V. MS **89,** 88–101.

Luo, Y., 1991. Calculation of wave paths for band-limited seismic waves, *Expanded Abstracts of the 1991 Technical Programme of the Society of Exploration Geophysicists with Biographies,* pp. 1509–1512, Society of Exploration Geophysicists, Oklahoma, USA.

Luo, Y. & Schuster, G.T., 1990. Wave equation traveltime inversion, *Expanded Abstracts of the 1990 Technical Programme of the Society of Exploration Geophysicists with Biographies,* pp. 1207–1210, Society of Exploration Geophysicists, Oklahoma, USA.

Luo, Y. & Schuster, G.T., 1991. Wave equation traveltime inversion, *Geophysics,* **56,** 645–653.

Marquering, H., Dahlen, F.A. & Nolet, G., 1999. Three-dimensional sensitivity kernels for finite-frequency traveltimes: the banana–doughnut paradox, *Geophys. J. Int.,* **137,** 805–815.

Ritsema, J., Van Heijst & Woodhouse, J., 1999. Complex shear wave velocity structure imaged beneath Africa and Iceland, *Science,* 1925–1928.

Schuster, G.T. & Hu, J., 2000. Green's function for migration: continuous recording geometry, *Geophysics,* **65,** 167–175.

Schuster, G.T., 1996. Resolution limits for crosswell migration and traveltime tomography, *Geophys. J. Int.,* **127,** 427–440.

Schuster, G.T. & Quintus-Bosz, A., 1993. Wave path eikonal traveltime inversion: Theory, *Geophysics,* **58,** 1314–1323.

Sheriff, R.E. & Geldart, L.P., 1982. *Exploration Seismology: History, Theory, and Data Acquisition,* Cambridge University Press, Cambridge.

Su, W., Woodward, R. & Dziewonski, A., 1994. Degree-12 model of shear velocity heterogeneity in the mantle, *J. geophys. Res.,* **99,** 6945–6980.

Tong, J., Dahlen, F.A., Nolet, G. & Marquering, H., 1998. Diffraction effects upon finite-frequency traveltimes: a simple 2-D example, *Geophys. Res. Lett.,* **25,** 1983–1986.

Vasco, D.W., Peterson, J.E. & Majer, E.L., 1995, Beyond ray tomography: Wave paths and Fresnel volumes, *Geophysics,* **60,** 1790–1804.

Woodward, M., 1989. Wave equation tomography, *PhD dissertation,* Stanford University, Stanford, CA, USA.

Woodward, M., 1992. Wave-equation tomography, *Geophysics,* **57,** 15–26.

Woodward, M. & Rocca, F., 1988. Wave-equation tomography, *58th Ann. Internat. Mtg., Soc. Explor. Geophys., Expanded Abstracts,* pp. 1232–1235.

Wu, R. & Toksoz, N., 1987. Diffraction tomography and multisource holography applied to seismic imaging, *Geophysics,* **52,** 11–25.

Zhou, C., Schuster, G.T., Hassanzadeh, S. & Harris, J.M., 1997. Elastic wave equation traveltime and waveform inversion of crosswell data, *Geophysics,* **62,** 853–868.

APPENDIX A: ASYMPTOTIC INVERSION

In this appendix we derive the asymptotic inversion eqs (5) and (9). We now consider the Fourier integral operator (FIO) defined by

$$\begin{aligned}(\mathrm{FO})(\mathbf{r}) = &-\frac{4}{(2\pi)^n}\int_0^{+\infty}\int_{\partial\mathbf{X}}\omega^{(n-3)/2}\,\mathrm{Im}[\Delta\phi(\omega,\mathbf{r}_\mathrm{s},\mathbf{r}_\mathrm{g})]\\ &\times\sin\left[\omega\tau(\mathbf{r},\mathbf{r}_\mathrm{s},\mathbf{r}_\mathrm{g})-\frac{(n+1)\pi}{4}\right]\\ &\times\frac{h(\mathbf{r},\mathbf{r}_\mathrm{s},\mathbf{r}_\mathrm{g})}{A(\mathbf{r},\mathbf{r}_\mathrm{s},\mathbf{r}_\mathrm{g})}\chi(\mathbf{r},\mathbf{r}_\mathrm{s},\mathbf{r}_\mathrm{g})\,d\mathbf{r}_\mathrm{g}\,d\omega. \qquad (A1)\end{aligned}$$

Substituting eq. (4) in eq. (A1) we rewrite F as

$$\begin{aligned}(\mathrm{FO})(\mathbf{r}) = &\frac{4}{(2\pi)^n}\int_0^{+\infty}\int_{\partial\mathbf{X}}\int_{\mathbf{X}}\omega^{n-1}\mathbf{O}(\mathbf{r}')A'(\mathbf{r},\mathbf{r}',\mathbf{r}_\mathrm{s},\mathbf{r}_\mathrm{g})\\ &\times\sin\left[\omega\tau(\mathbf{r},\mathbf{r}_\mathrm{s},\mathbf{r}_\mathrm{g})-\frac{(n+1)\pi}{4}\right]\\ &\times\sin\left[\omega\tau(\mathbf{r}',\mathbf{r}_\mathrm{s},\mathbf{r}_\mathrm{g})-\frac{(n+1)\pi}{4}\right]\\ &\times h(\mathbf{r},\mathbf{r}_\mathrm{s},\mathbf{r}_\mathrm{g})\chi(\mathbf{r},\mathbf{r}_\mathrm{s},\mathbf{r}_\mathrm{g})\,d\mathbf{r}'\,d\mathbf{r}_\mathrm{g}\,d\omega, \qquad (A2)\end{aligned}$$

where $A'(\mathbf{r},\mathbf{r}',\mathbf{r}_\mathrm{s},\mathbf{r}_\mathrm{g}) = \frac{A(\mathbf{r}',\mathbf{r}_\mathrm{s},\mathbf{r}_\mathrm{g})}{A(\mathbf{r},\mathbf{r}_\mathrm{s},\mathbf{r}_\mathrm{g})}$. Since both $\tau(\mathbf{r},\mathbf{r}_\mathrm{s},\mathbf{r}_\mathrm{g})$ and $\tau(\mathbf{r}',\mathbf{r}_\mathrm{s},\mathbf{r}_\mathrm{g})$ are non-negative, we rewrite the FIO as

$$\begin{aligned}(\mathrm{FO})(\mathbf{r}) = &\frac{1}{(2\pi)^n}\int_{-\infty}^{+\infty}\int_{\partial\mathbf{X}}\int_{\mathbf{X}}\omega^{n-1}\mathbf{O}(\mathbf{r}')A'(\mathbf{r},\mathbf{r}',\mathbf{r}_\mathrm{s},\mathbf{r}_\mathrm{g})\\ &\times\exp\{i\omega[\tau(\mathbf{r}',\mathbf{r}_\mathrm{s},\mathbf{r}_\mathrm{g})-\tau(\mathbf{r},\mathbf{r}_\mathrm{s},\mathbf{r}_\mathrm{g})]\}\\ &\times h(\mathbf{r},\mathbf{r}_\mathrm{s},\mathbf{r}_\mathrm{g})\chi(\mathbf{r},\mathbf{r}_\mathrm{s},\mathbf{r}_\mathrm{g})\,d\mathbf{r}'\,d\mathbf{r}_\mathrm{g}\,d\omega. \qquad (A3)\end{aligned}$$

According to Beylkin's theory (Beylkin 1985), the FIO in (A3) is a pseudodifferential operator, and by making use only of its first-order term we have

$$\begin{aligned}(\mathrm{FO})(\mathbf{r}) \sim &\frac{1}{(2\pi)^n}\int_{-\infty}^{+\infty}\int_{\partial\mathbf{X}}\int_{\mathbf{X}}\omega^{n-1}\mathbf{O}(\mathbf{r}')\\ &\times\mathrm{e}^{i\omega\nabla_\mathbf{r}\tau(\mathbf{r},\mathbf{r}_\mathrm{s},\mathbf{r}_\mathrm{g})\cdot(\mathbf{r}'-\mathbf{r})}\\ &\times h(\mathbf{r},\mathbf{r}_\mathrm{s},\mathbf{r}_\mathrm{g})\chi(\mathbf{r},\mathbf{r}_\mathrm{s},\mathbf{r}_\mathrm{g})\,d\mathbf{r}'\,d\mathbf{r}_\mathrm{g}\,d\omega. \qquad (A4)\end{aligned}$$

Changing variables of integration from ω, $\mathbf{r}_\mathrm{g}$ to $\mathbf{k}$, where

$$\mathbf{k} = \omega\nabla_\mathbf{r}\tau(\mathbf{r},\mathbf{r}_\mathrm{s},\mathbf{r}_\mathrm{g}), \qquad (A5)$$

we have

$$d\mathbf{k} = \omega^{n-1}h(\mathbf{r},\mathbf{r}_\mathrm{s},\mathbf{r}_\mathrm{g})\,d\mathbf{r}_\mathrm{g}\,d\omega, \qquad (A6)$$

and

$$\begin{aligned}(\mathrm{FO})(\mathbf{r}) &\sim \frac{1}{(2\pi)^n}\int_{\Omega(\mathbf{r})}\int_{\mathbf{X}}\mathrm{e}^{i\mathbf{k}\cdot(\mathbf{r}'-\mathbf{r})}\mathbf{O}(\mathbf{r}')\,d\mathbf{r}'\,d\mathbf{k}\\ &= \frac{1}{(2\pi)^n}\int_{\Omega(\mathbf{r})}\mathrm{e}^{-i\mathbf{k}\cdot\mathbf{r}}\hat{\mathbf{O}}(\mathbf{k})\,d\mathbf{k}, \qquad (A7)\end{aligned}$$

where $\hat{\mathbf{O}}(\mathbf{k})$ is the Fourier transform of the object function $\mathbf{O}(\mathbf{r})$; the Fourier domain $\Omega(\mathbf{r})$ is determined by the frequency range and by those source–receiver pairs $\eta_{\mathrm{sg}}(\mathbf{r})$ for which the associated wave path

and the recorded traveltimes can be influenced by the perturbation at **r**. The domain of $\Omega(\mathbf{r})$ determines the spatial resolution of the reconstructed object function and controls what can be recovered (Beylkin 1985).

Thus from (A7) we obtain an approximate reconstruction formula (5), and its Fourier transform (9). Substituting $\mathrm{Im}[\Delta\phi(\omega, \mathbf{r}_s, \mathbf{r}_g)] \approx \omega\Delta\tau\left(\mathbf{r}_s, \mathbf{r}_g\right)$ into the above derivation, eq. (8) can be obtained directly.

APPENDIX B: THE MAXIMUM WAVENUMBERS FOR DIVING-WAVE TRAVELTIME TOMOGRAPHY

In this appendix, formulae are derived for the maximum wavenumbers for diving-wave traveltime tomography, eqs (15) and (16) in the text.

According to Sheriff & Geldart (1982), in the case of a linear increase of velocity with depth, $v = v_0 + az$, the raypath from a source point **s** to some receiver point **g** is a circular arc with the centre on the line located v_0/a above the surface. Therefore,

$$\tau_{\mathbf{sg}} = \frac{2}{a}\ln\left[\frac{ax_{\mathbf{sg}}}{2v_0} + \sqrt{1+\left(\frac{ax_{\mathbf{sg}}}{2v_0}\right)^2}\right], \tag{B8}$$

where $\tau_{\mathbf{sg}}$ denotes the first arrival traveltime for the raypath **sg**, x_{sg} denotes the horizontal distance between **s** and **g**, and both the source and receiver are at the surface.

For some point **x** on the raypath **sg**, we have

$$\tau_{\mathbf{xg}} = \frac{1}{a}\left(c\ln\frac{p_{\mathbf{xg}}v}{1+\sqrt{1-p_{\mathbf{xg}}^2v^2}} - \ln\frac{p_{\mathbf{xg}}v_0}{1+\sqrt{1-p_{\mathbf{xg}}^2v_0^2}}\right), \tag{B9}$$

where $\tau_{\mathbf{xg}}$ denotes the first arrival traveltime for the raypath **xg**, v is the velocity at the point **x**; c is determined such that, when $x_{\mathbf{xg}} \le x_{\mathbf{sg}}/2$, $c = 1$, and when $x_{\mathbf{xg}} \ge x_{\mathbf{sg}}/2$, $c = -1$, where $x_{\mathbf{xg}}$ denotes the horizontal distance between **x** and **g**; and $p_{\mathbf{xg}}$ is the raypath parameter that can be expressed as

$$p_{\mathbf{xg}} = \frac{1}{\sqrt{v_0^2 + \left\{\left[a\left(x_{\mathbf{xg}}^2+z^2\right)+2zv_0\right]/2x_{\mathbf{xg}}\right\}^2}}. \tag{B10}$$

For a fixed source at **s**, an image point at **x**, and the ray leaving at **s** returns to the surface through **x** at receiver **g**, the maximum wavenumbers can be obtained at the receiver $\mathbf{g}'$ close to **g** such that the image point **x** is on the boundary of the wave path associated with the source–receiver pair ($\mathbf{s}$, $\mathbf{g}'$), that is,

$$|\tau_{\mathbf{sx}} + \tau_{\mathbf{xg}'} - \tau_{\mathbf{sg}'}| = \frac{T}{2}, \tag{B11}$$

where $\tau_{\mathbf{sg}'}$ denotes the first arrival traveltime from **s** to $\mathbf{g}'$.

$\tau_{\mathbf{xg}'}$ can be approximated by a Taylor series up to second order as,

$$\tau_{\mathbf{xg}'} \approx \tau_{\mathbf{xg}} + p(\Delta x_{\mathbf{gg}'}) + c\frac{(\Delta x_{\mathbf{gg}'})^2}{2}\frac{ap^2}{\sqrt{1-p^2v_0^2}-c\sqrt{1-p^2v^2}} \times\sqrt{1-p^2v_0^2}\sqrt{1-p^2v^2}, \tag{B12}$$

where p denotes the ray parameter of the raypath **sxg** and $\Delta x_{\mathbf{gg}'}$ denotes the x-coordinate difference between **g** and $\mathbf{g}'$.

Similarly, $\tau_{\mathbf{sg}'}$ can be approximated as,

$$\tau_{\mathbf{sg}'} \approx \tau_{\mathbf{sg}} + p(\Delta x_{\mathbf{gg}'}) - \frac{(x_{\mathbf{gg}'})^2}{2}\frac{ap^2}{2}\sqrt{1-p^2v_0^2}. \tag{B13}$$

From eqs (B11) to(B13), we have

$$|\Delta x_{\mathbf{gg}'}| \approx \sqrt{\frac{2T}{ap^2\sqrt{1-p^2v_0^2}}\frac{\sqrt{1-p^2v_0^2}-c\sqrt{1-p^2v^2}}{\sqrt{1-p^2v_0^2}+c\sqrt{1-p^2v^2}}}. \tag{B14}$$

Inserting eq. (B12) into eq. (10) yields

$$|k_x| = \frac{2\pi}{T}\left|\frac{\partial(\tau_{\mathbf{sx}}+\tau_{\mathbf{xg}'})}{\partial x}\right| \approx \frac{2\pi}{T}\left|\frac{\partial(\tau_{\mathbf{sx}}+\tau_{\mathbf{xg}}+p\Delta x_{\mathbf{gg}'})}{\partial x}\right| = \frac{2\pi}{T}\left|\frac{\partial(p\Delta x_{\mathbf{gg}'})}{\partial x}\right| = \frac{2\pi}{T}\left|\frac{\partial p}{\partial x}\right||\Delta x_{\mathbf{gg}'}|, \tag{B15}$$

and similarly,

$$|k_z| \approx \frac{2\pi}{T}\left|\frac{\partial p}{\partial z}\right||\Delta x_{\mathbf{gg}'}|, \tag{B16}$$

where $\nabla(\tau_{sx}+\tau_{xg}) = 0$, since **x** is on the raypath **sg**; $|\partial p/\partial x|$ and $\partial p/\partial z|$ can be derived from eq. (B10) as

$$\left|\frac{\partial p}{\partial x}\right| = \frac{ap^2\sqrt{1-p^2v_0^2}\sqrt{1-p^2v^2}}{\sqrt{1-p^2v_0^2}-c\sqrt{1-p^2v^2}}, \tag{B17}$$

and

$$\left|\frac{\partial p}{\partial z}\right| = \frac{ap^3v\sqrt{1-p^2v_0^2}}{\sqrt{1-p^2v_0^2}-c\sqrt{1-p^2v^2}}. \tag{B18}$$

Inserting eqs (B14), (B17) and (B18) into eqs (B15)–(B16) yields eqs (15) and (16).